

## Some interactions between small numbers of baroclinic, geostrophic vortices

W. R. Young

To cite this article: W. R. Young (1985) Some interactions between small numbers of baroclinic, geostrophic vortices, *Geophysical & Astrophysical Fluid Dynamics*, 33:1-4, 35-61, DOI: [10.1080/03091928508245422](https://doi.org/10.1080/03091928508245422)

To link to this article: <https://doi.org/10.1080/03091928508245422>



Published online: 01 Dec 2006.



Submit your article to this journal [↗](#)



Article views: 13



Citing articles: 16 [View citing articles](#) [↗](#)

# Some Interactions Between Small Numbers of Baroclinic, Geostrophic Vortices

W. R. YOUNG†

*Marine Physical Laboratory of the Scripps Institution of Oceanography,  
University of California, San Diego La Jolla, CA 92093*

*(Received June 19, 1984; in final form February 1, 1985)*

Various interactions between small numbers (two and four) of baroclinic, geostrophic point vortices in a two-layer system are studied with attention to the qualitative changes in behavior which occur as size of the deformation radius is varied.

A particularly interesting interaction, which illustrates the richness of baroclinic vortex dynamics, is a collision between two *hetons*. (A heton is a vortex pair in which the constituent vortices have opposite signs and are in opposite layers. The “breadth” of a heton is the distance between its constituent vortices. A translating heton transports heat.) When two hetons, which initially have different breadths, collide, the result is either an exchange of partners, or a “slip-through” collision in which the initial structures are preserved. It is shown here that the outcome is always an exchange, provided the deformation radius is sufficiently small. This strongly contrasts with a collision between pairs of classical, one-layer vortices in which no exchange occurs if the initial ratio of the breadths is sufficiently extreme.

Finally the transport of passive fluid by a translating baroclinic pair is investigated. A pair of vortices in the top layer transports no lower layer fluid if the distance between the vortices is less than 1.72 deformation radii. By contrast, the size of the region trapped by a heton increases without bound as the spacing between the vortices increases.

## 1. INTRODUCTION

Hogg and Stommel (1984a, b) have recently discussed the dynamics of discrete, baroclinic, point-vortices. These entities are exact so-

---

†Present address: Dept. of Earth Atmospheric and Planetary Sciences, Massachusetts Institute of Technology, Cambridge, MA 02139.

olutions of the two-layer,  $f$ -plane quasigeostrophic potential vorticity equation:

$$q_n + J(\psi_n, q_n) = 0, \quad (1.1)$$

where  $n=1, 2$  corresponds to the top, bottom layer and the potential vorticity is related to the streamfunction by:

$$q_n = \nabla^2 \psi_n + (-1)^n \frac{1}{2} \lambda^{-2} (\psi_1 - \psi_2). \quad (1.2)$$

For a detailed derivation of (1.1), see Pedlosky (1979).

The one layer ("barotropic") discrete vortices are well known, elegant examples of vortical motion (e.g. Lamb, 1932; Batchelor, 1967) and can be obtained by taking the limit  $\lambda \rightarrow 0$  in (1.1) and (1.2). Aref (1983) is an excellent, recent review of the barotropic problem.

This note supplements Hogg and Stommel's numerical and impressionistic account by: deriving the baroclinic generalization of the conservation laws, characterizing the motion passive particles in the velocity field of two baroclinic vortices, and discussing a particular four vortex interaction which is analytically accessible because the initial condition has a symmetry which is preserved in the ensuing quadrille. This last is a baroclinic analog of Love's (1894) study. Thus this is a catalog of the simplest properties of baroclinic point vortices: no direct geophysical applications are presented. However because of the  $f$ -plane quasigeostrophic potential vorticity equation (1.1) is central to oceanography and meteorology, a discussion of some elementary exact nonlinear solutions is of geophysical interest. In any case this is a prerequisite to a systematic exploration of the point vortex idealization.

Before turning to the derivation of the conservation laws note that the streamfunction associated with a point vortex of strength  $2\pi s_1$  in the *upper layer* is obtained by solving

$$\nabla^2 \psi_1 + \frac{1}{2} \lambda^{-2} (\psi_2 - \psi_1) = 2\pi s_1 \delta(\mathbf{x}), \quad \nabla^2 \psi_2 + \frac{1}{2} \lambda^{-2} (\psi_1 - \psi_2) = 0. \quad (1.3)$$

The solution is

$$\psi_1 = \frac{1}{2} s_1 \{ \ln r - K_0(r/\lambda) \}, \quad \psi_2 = \frac{1}{2} s_1 \{ \ln r + K_0(r/\lambda) \} \quad (1.4)$$

and the streamfunction produced by a vortex of strength  $2\pi s_2$  in the lower layer is

$$\psi_1 = \frac{1}{2}s_2\{\ln r + K_0(r/\lambda)\}, \quad \psi_2 = \frac{1}{2}s_2\{\ln r - K_0(r/\lambda)\}. \quad (1.5)$$

The streamfunction produced by an ensemble of vortices is calculated from (1.4) and (1.5) by linear superposition.

The streamfunctions in (1.4) are shown graphically in Figure 1A and the azimuthal velocities,  $\partial\psi_n/\partial r$ , are shown in Figure 1.B. The lower layer azimuthal velocity is a maximum at  $r/\lambda = 1.114$ .

## 2. CONSERVATION LAWS

The conservation laws can be derived directly from (1.1). The derivations are straightforward generalizations of those in Batchelor (1967). The most obvious conservation laws are:

$$(d/dt) \int q_1 dA = 0, \quad (d/dt) \int q_2 dA = 0, \quad (2.1)$$

the integral being taken over the whole plane.

We can also obtain simple expressions for the first integral moments of the potential vorticity distributions:

$$(d/dt) \int x q_1 dA = \frac{1}{2}\lambda^{-2} \int \psi_{1y} \psi_2 dA,$$

$$(d/dt) \int x q_2 dA = \frac{1}{2}\lambda^{-2} \int \psi_{2y} \psi_1 dA.$$

Adding the above gives another integral invariant,

$$(d/dt) \int x(q_1 + q_2) dA = 0, \quad (2.2)$$

and similarly

$$(d/dt) \int y(q_1 + q_2) dA = 0. \quad (2.3)$$

Using the above we define the "center of vorticity":

$$X \equiv \int x(q_1 + q_2) dA / \int (q_1 + q_2) dA,$$

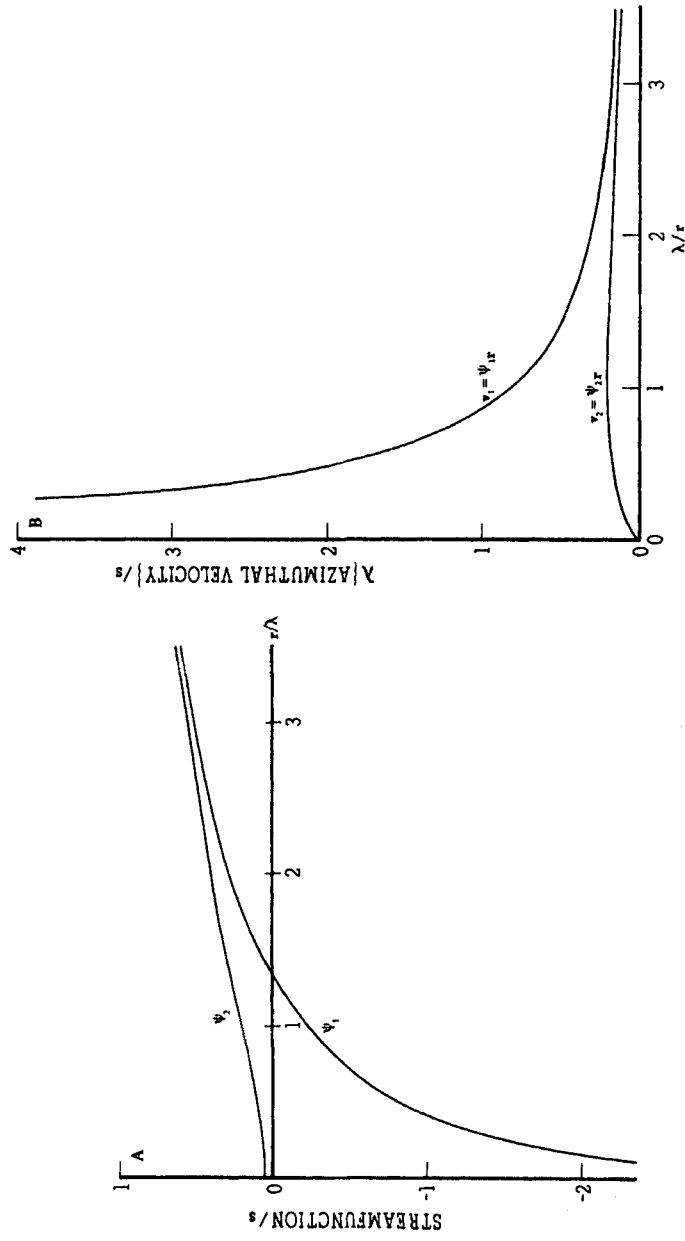


FIGURE 1 (A) The streamfunction defined in (1.4). (B) The azimuthal velocity associated with a vortex in the upper layer. The lower layer velocity has a maximum at  $r/\lambda = 1.114$ .

$$Y \equiv \int y(q_1 + q_2) dA / \int (q_1 + q_2) dA. \quad (2.4)$$

If  $\int (q_1 + q_2) dA = 0$  then the center is at infinity.

The second integral moments satisfy

$$\begin{aligned} (d/dt) \int (x^2 + y^2) q_1 dA &= \lambda^{-2} \int (x\psi_{1y} + y\psi_{1x}) \psi_2 dA, \\ (d/dt) \int (x^2 + y^2) q_2 dA &= \lambda^{-2} \int (x\psi_{2y} + y\psi_{2x}) \psi_1 dA, \end{aligned} \quad (2.5)$$

and once again addition gives a conservation law:

$$(d/dt) \int (x^2 + y^2)(q_1 + q_2) dA = 0. \quad (2.6)$$

Thus the length,

$$D^2 \equiv \int \{(x - X)^2 + (y - Y)^2\} (q_1 + q_2) dA / \int (q_1 + q_2) dA, \quad (2.7)$$

is a constant, i.e. the dispersion of the vorticity distribution about its center is an invariant.

Finally, there is energy conservation and, as in the barotropic case, there is a difficulty associated with the slow decay of the streamfunction at infinity. The correct definition is

$$W = -\frac{1}{2} \int (\psi_1 q_1 + \psi_2 q_2) dA \quad (2.8)$$

and direct calculation shows this is invariant.

The derivations above apply to arbitrary distributions of  $q_1$  and  $q_2$ . To obtain the appropriate expressions for an ensemble of point vortices of strengths  $2\pi s_1, 2\pi s_2, \dots, 2\pi s_m$  at the points  $\mathbf{x}_1, \mathbf{x}_2, \dots, \mathbf{x}_m$  in the upper layer and strengths  $2\pi s_{m+1}, \dots, 2\pi s_{n+m}$  at points  $\mathbf{x}_{m+1}, \dots, \mathbf{x}_{m+n}$  in the lower layer substitute:

$$q_1 = 2\pi \sum_{p=1}^m s_p \delta(\mathbf{x} - \mathbf{x}_p), \quad q_2 = 2\pi \sum_{p=m}^{n+m} s_p \delta(\mathbf{x} - \mathbf{x}_p) \quad (2.9)$$

into (2.2), (2.3), (2.6) and (2.8).

### 3. MOTION OF TWO POINT VORTICES

#### Two vortices in the upper layer

Suppose that the two vortices are in the upper layer. Then the distance between them,  $d=2a$ , remains constant. If  $s_1 + s_2$  is nonzero vortices move in a circular path about the center of vorticity with angular velocity.

$$\omega = \frac{1}{2}d^{-2}(s_1 + s_2)G^+(d/\lambda), \quad G^+(z) = 1 + zK_1(z). \quad (3.1)$$

If  $s_1 + s_2 = 0$  then the center of vorticity is at infinity and the pair translates at a speed

$$c = \frac{1}{2}d^{-1}sG^+(d/\lambda). \quad (3.2)$$

To visualize the flow associated with this pair we use a coordinate system translating with the vortices. In this frame the motion is steady and the streamfunctions are

$$\chi_1 = cy + \frac{1}{2}s \ln(r_1/r_2) + \frac{1}{2}s\{K_0(r_2/\lambda) - K_0(r_1/\lambda)\}, \quad (3.3)$$

$$\chi_2 = cy + \frac{1}{2}s \ln(r_1/r_2) - \frac{1}{2}s\{K_0(r_2/\lambda) - K_0(r_1/\lambda)\},$$

where

$$r_1 = [x^2 + (y-a)^2]^{1/2}, \quad r_2 = [x^2 + (y+a)^2]^{1/2}, \quad (3.4)$$

are the distances from the two vortices at  $(0, \pm a)$  and  $s_1 = -s_2 = s$ . Note that  $\chi_n$  changes sign if  $y \rightarrow -y$ . The functions  $\chi$  will be referred to as "streakfunctions".

A sketch of  $\chi_n$  is shown in Figure 2. As in the barotropic case discussed by Lamb (1932), the fluid enclosed by the oval  $\chi_n = 0$  migrates with the vortex pair whilst the external fluid is subject to a finite displacement. The size of the trapped region may be gauged from Figures 3 and 4.

Figure 3 shows the streamfunctions  $\chi_n$  evaluated along the axis CD in Figure 2. The semi-major axis of the oval in Figure 2 corresponds to the intersection of these curves with the horizontal axis. In the upper layer this is always at a distance slightly greater than  $2a$  no

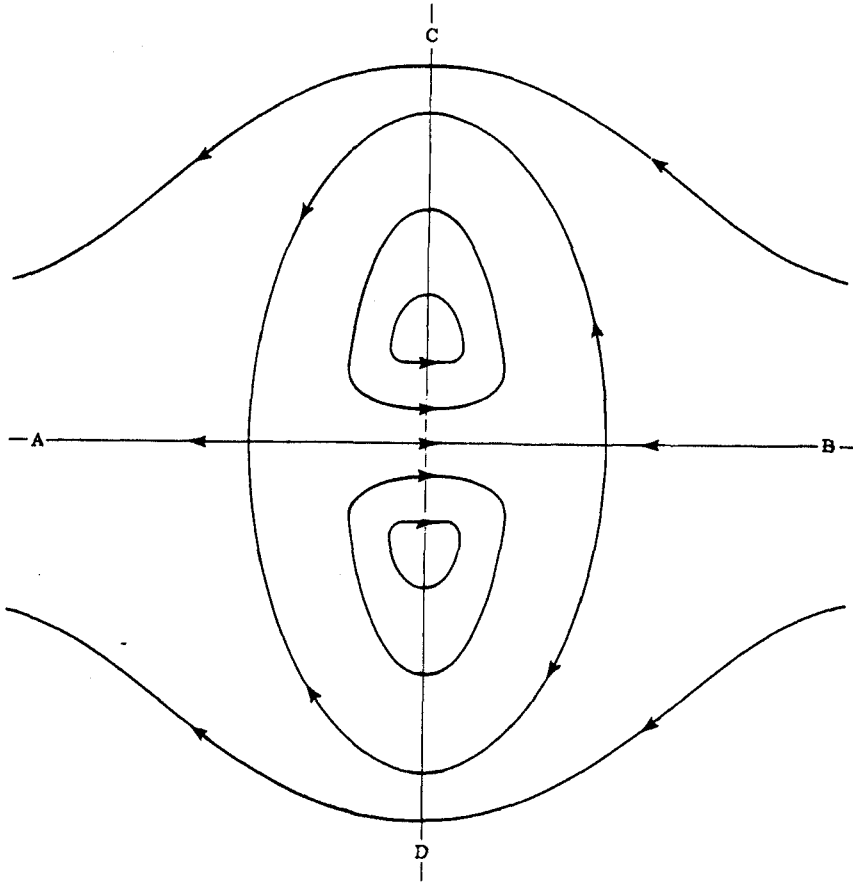


FIGURE 2 A schematic illustration of the streamfunctions defined in (3.3). The fluid inside the oval is transported with the travelling pair.

matter how many deformation radii separate the two vortices. In the lower layer however, the size of the oval is sensitive to  $a/\lambda$ . When this parameter is large the trapped region in the lower layer is only a little smaller than that in the upper layer, and is coincident with it (e.g. Figure 3C). As  $a/\lambda$  decreases the trapped region in the lower layer shrinks relative to that in the upper (e.g. Figure 3B). When  $a/\lambda=0.860$  the lower layer oval disappears entirely and no lower layer fluid is transported by the pair (e.g. Figure 3A).

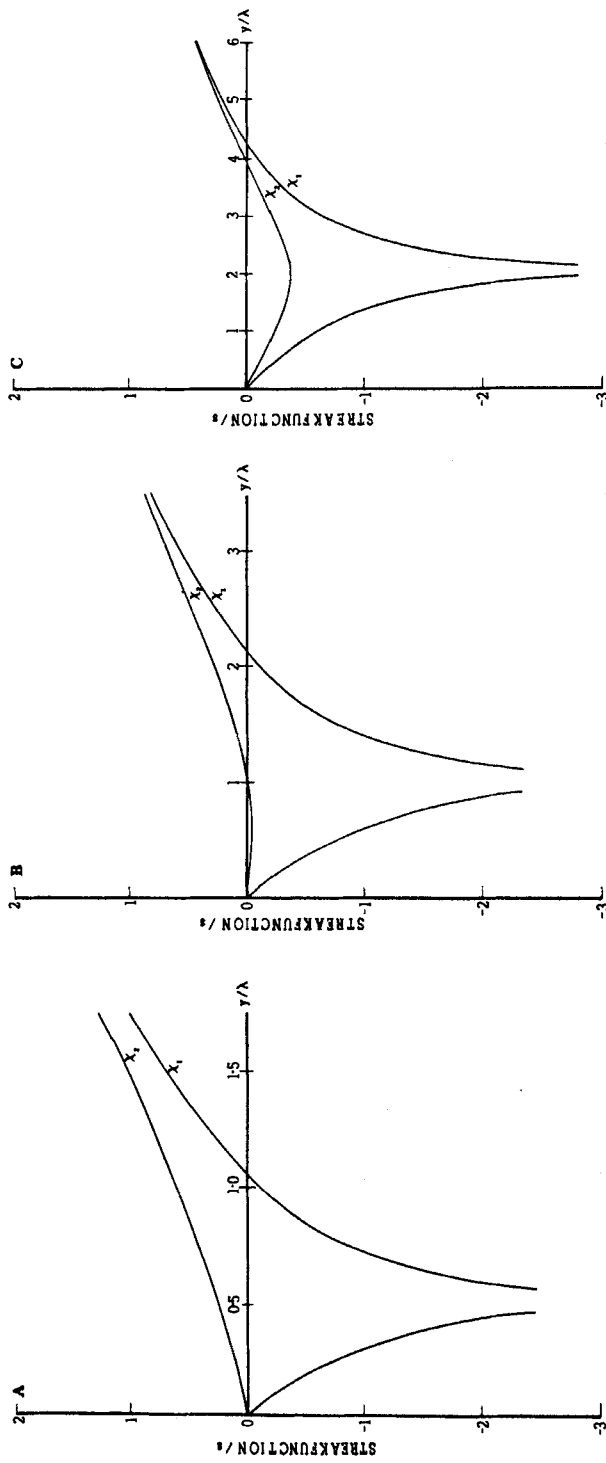


FIGURE 3 The streamfunctions evaluated along the axis CD in Figure 2 with various values of  $d/\lambda$ : (A)  $d/\lambda = 1$ , (B)  $d/\lambda = 2$ , (C)  $d/\lambda = 4$ . When  $d/\lambda$  is less than 1.72 there is no  $\xi_2 = 0$  contour and consequently no lower layer fluid is transported.

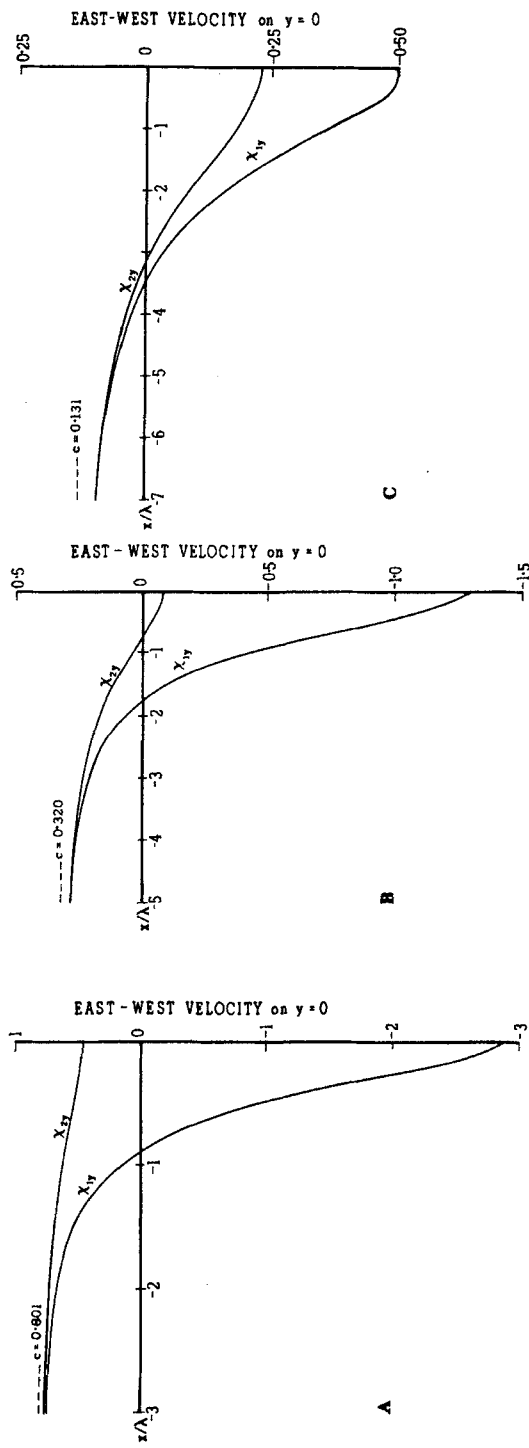


FIGURE 4 East-West velocity evaluated along the axis AB in Figure 2 with various values of  $d/\lambda$ : (A)  $d/\lambda = 1$ , (B)  $d/\lambda = 2$ , (C)  $d/\lambda = 4$ .

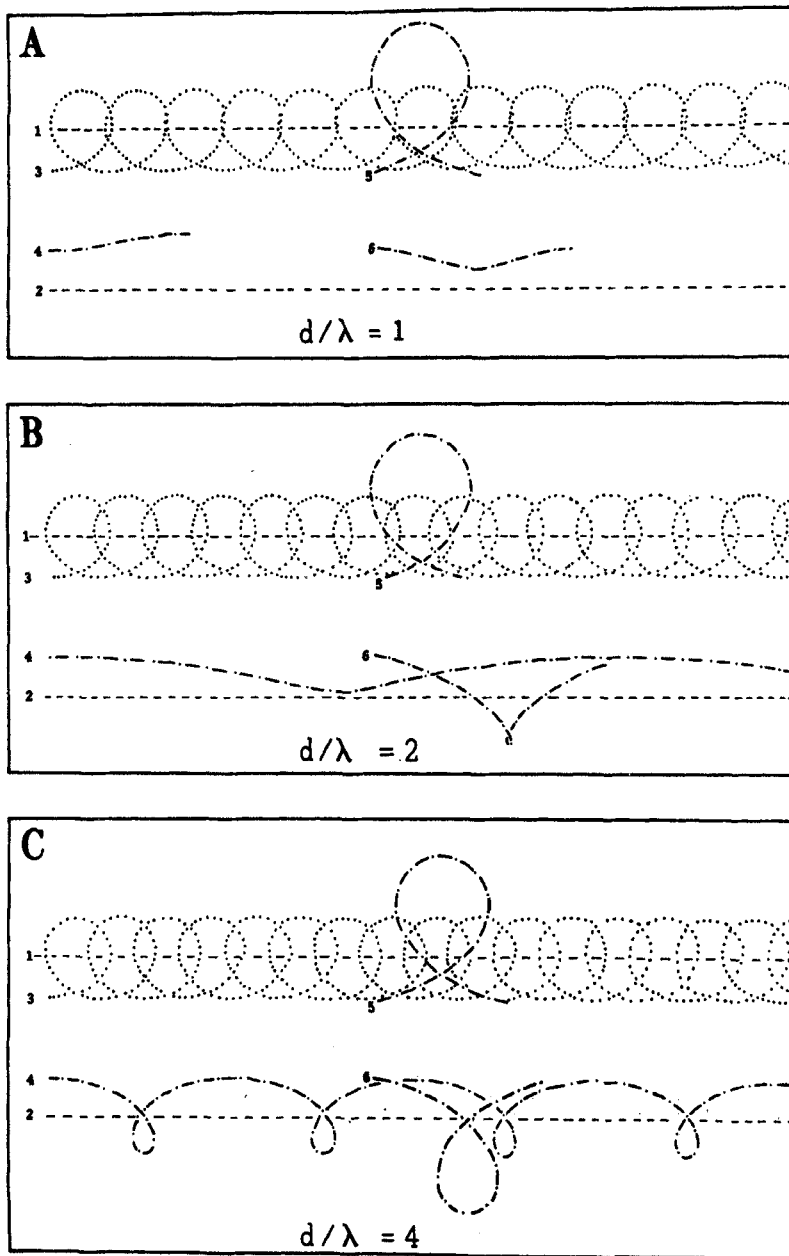


FIGURE 5 Results of a numerical integration of the equations of motion in a stationary frame of reference. There are six vortices (four of which have zero strength) and their initial positions are indicated by the numbers. Vortices 1 and 2 have strengths  $+1$  and  $-1$  respectively, and are both in the top layer. The passive markers 3 and 5 are in the top layer while 4 and 6 are in the bottom. Note especially the behavior of 4 as  $d/\lambda$  is varied.

Figure 4 shows the east-west velocity,  $-\chi_{xy}$ , along the axis AB in Figure 2. The semi-minor axis of the oval corresponds to the intersection of these curves with the horizontal axis. When  $a/\lambda$  is large the two ovals coincide and the semi-minor axis approaches  $3^{1/2}a$ . As  $a/\lambda$  decreases the semi-minor axis in the upper layer approaches  $2a$  while the lower layer oval disappears when  $a/\lambda$  is less than 0.860.

The absence of lower layer trapping when the vortices are closer than  $1.720 \lambda$  occurs because the lower layer velocities are feeble in the neighborhood of the singularity (Figure 1B) and trapping requires velocities *between* the vortices which are strong enough to oppose the speed of translation of the system.

Finally in Figure 5 shows a numerical integration of the equations of motion in a *stationary* frame of reference where the top-pair translates from left to right. Four vortices of zero strength (i.e. passive markers) are released so that the disturbance created by the passage of the surface pair can be visualized. This experiment visually reinforces the analytic conclusions obtained from (3.3). In particular it shows that the fluid in the lower layer is only slightly disturbed when the top pair is separated by less than about one deformation radius.

### Two vortices in different layers

Next we examine the interaction of two vortices in different layers. Hogg and Stommel (1984) noted that when the vortices also have opposite signs then the migrating pair transports heat. They coined the term "heton" to denote this particular combination.

Once again, because of the integral constraints,  $d=2a$  is constant. If  $s_1 + s_2$  is nonzero then the vortices move in a circular path about the center of vorticity with angular velocity.

$$\omega = \frac{1}{2}d^{-2}(s_1 + s_2)G^-(d/\lambda), \quad G^-(z) = 1 - zK_1(z). \quad (3.5)$$

If  $s_1 + s_2$  is zero then the pair translates with a speed

$$c = \frac{1}{2}d^{-1}sG^-(d/\lambda). \quad (3.6)$$

In a frame of reference moving with the pair the motion is steady

and the streamfunctions are

$$\begin{aligned}\chi_1 &= cy + \frac{1}{2}s \ln(r_1/r_2) - \frac{1}{2}s\{K_0(r_1/d) + K_0(r_2/d)\}, \\ \chi_2 &= cy + \frac{1}{2}s \ln(r_1/r_2) + \frac{1}{2}s\{K_0(r_1/d) + K_0(r_2/d)\},\end{aligned}\tag{3.7}$$

where  $r_1$  and  $r_2$  are defined in (3.4) and the positive vortex of strength  $s > 0$  is at  $y = a$  in the upper layer. The streamfunctions in (3.7) are no longer antisymmetric under reflection through the  $x$ -axis. In this case however

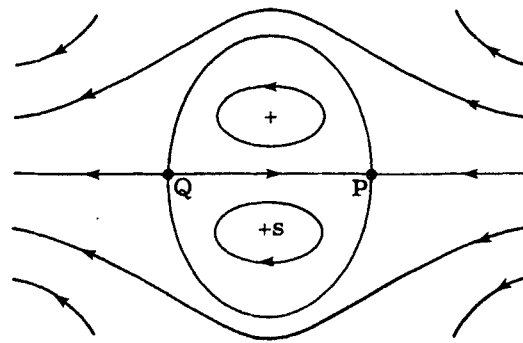
$$\chi_1(x, y, t) = -\chi_2(x, -y, t),\tag{3.8}$$

so to visualize the flow it is only necessary to plot  $\chi_1$ .

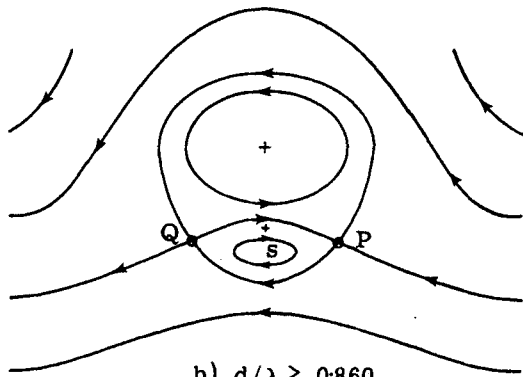
Begin by noting that when  $d/\lambda$  is very large we must have a pattern very like that in Figure 2 because the flow is almost barotropic except in the immediate vicinity of the vortices. However the structure of the flow alters as  $d/\lambda$  is decreased—see Figure 6. The most dramatic change occurs when  $d/\lambda = 0.860$ . At this critical separation the clockwise cell is overwhelmed by the counterclockwise cell and there is only one region of closed streamlines which is centered on the vortex at  $y = a$ . These results follow analytically from a local analysis of the flow field in the vicinity of the stagnation point,  $S$ , in Figure 6. This shows that when  $d/\lambda$  is less than 0.860 the streamlines are hyperbolic in the neighborhood while when  $d/\lambda$  is greater than 0.860 they are elliptical.

Figure 7 shows the position of the point  $S$ ,  $(0, y_s)$ , as a function of the separation of the vortices. As the separation goes to zero,  $|y_s| \rightarrow \infty$  and the region of counterclockwise recirculation expands indefinitely. This unbounded growth of the trapped region is a consequence of the slow translation of a heton when the vortices are close together. In this limit the configuration moves so slowly that the weak, far-field velocities, induced by the vortices, are sufficient to drag fluid along with the pair. This argument helps explain Hogg and Stommel's observation that heat transport is a maximum when the breadth of a heton vanishes.

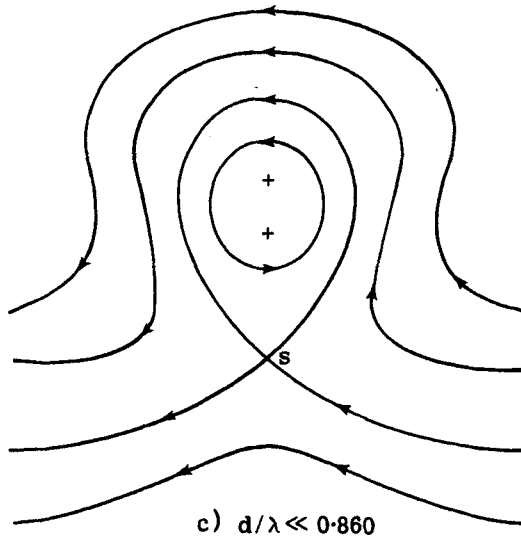
Figure 8 shows a numerical integration of the equations of motion in a stationary frame of reference. The heton is composed of vortices 1 and 2 while 3, 4 and 5 are passive markers which illustrate the



a)  $d/\lambda \gg 1$



b)  $d/\lambda \geq 0.860$



c)  $d/\lambda \ll 0.860$

FIGURE 6 A schematic illustration of the changes in form of  $\chi_1$  in (3.7) as  $d/\lambda$  is varied. The point where  $\partial\chi_1/\partial y=0$  is denoted by S. When  $d/\lambda < 0.860$  this point is a saddle and if the inequality is reversed it is a center.

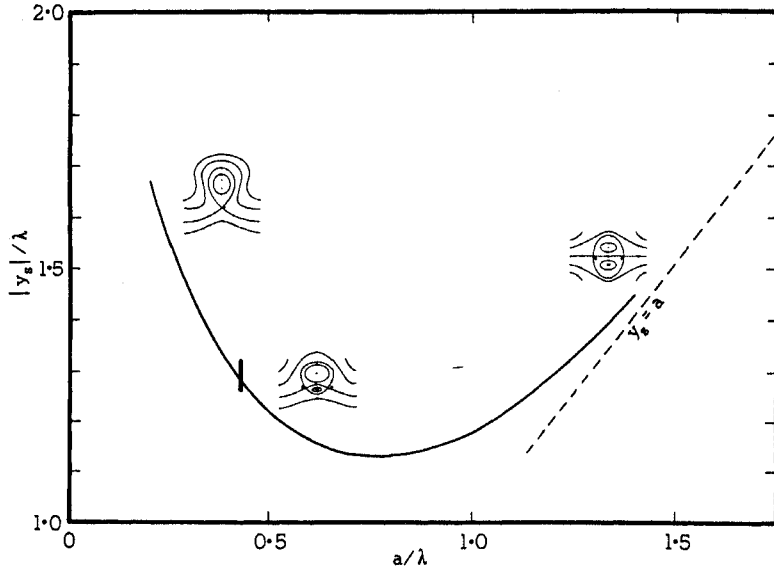


FIGURE 7 The position of the point  $S$ ,  $y_s$ , as a function of the separation,  $d = 2a$ , of the vortices. At large separations  $S$  is a center and it coincides with the lower layer vortex. At small separations  $S$  is a hyperbolic point and  $y_s$  approaches negative infinity as  $\ln(a/\lambda)$ .

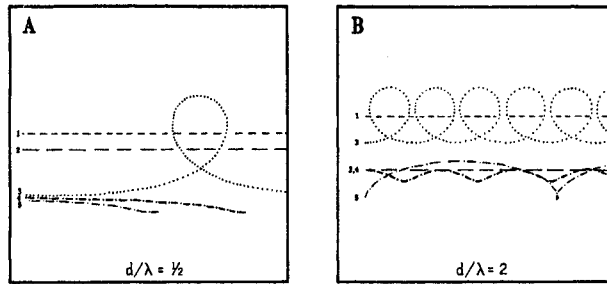


FIGURE 8 A numerical integration in a stationary frame of reference. The initial positions of the vortices are indicated by their labels. Vortex 1 has strength  $+1$  and is in the top layer while vortex 2 has strength  $-1$  and is in the bottom layer. The other three vortices are all in the top layer and have zero strength. (A) This figure shows the large extent of the trapped region when  $d/\lambda$  is small. (B) This figure shows that the clockwise circulation associated with vortex 2 is much weaker, and less extensive, than the counterclockwise circulation associated with vortex 1.

disturbance. Figure 8A shows that in the limit of small  $d/\lambda$  the region of trapped fluid is much larger than  $d$ .

#### 4. MOTION OF FOUR POINT VORTICES

In this section I shall discuss some special solutions of the four vortex problem. This is an attempt to develop intuition about the strength of the bond which unites two vortices into a heton. For instance, if two hetons collide do the initial pairings survive or is there an exchange of partners? Questions such as this can be resolved with the class of solutions discussed in this section.

The barotropic problem which suggested the investigation below was discussed by Love (1894) and, in greater generality, by Acton (1976). The idea is to find a four-vortex solution which is tractable because a symmetry in the initial conditions is preserved in the subsequent motion.

Begin by considering two vortices of strength  $s_0$  and  $s_1$  (the "original" vortices). One now constructs image vortices by reflecting the original vortices in an arbitrary line, which I suppose is the  $x$ -axis. The image vortex has the opposite sign of the original. If the image is in the same layer as the original the configuration will be referred to as "strongly symmetric" (see Figure 9A). In this case both streamfunctions are antisymmetric about the axis of reflection and this line is a streamline. Alternatively it is possible to place the images in different layers than the originals. This configuration will be referred to as "weakly symmetric" (see Figure 9B). In this case the streamfunctions have the property (3.8) and the axis of reflection is not a streamline.

It is perhaps, not initially obvious that the weakly symmetric configuration is preserved. The easiest way to convince one's self of this is to note that the velocity of vortex A in Figure 9B is obtained from the vector sum of the velocities induced by vortices B, C and D. Likewise one can geometrically construct the velocity of vortex B and easily see that the tendency is for these two vortices to remain equidistant from the axis of symmetry.

Besides the division into strongly and weakly symmetric there is a further distinction according to whether the two original vortices are in the same or different layers.

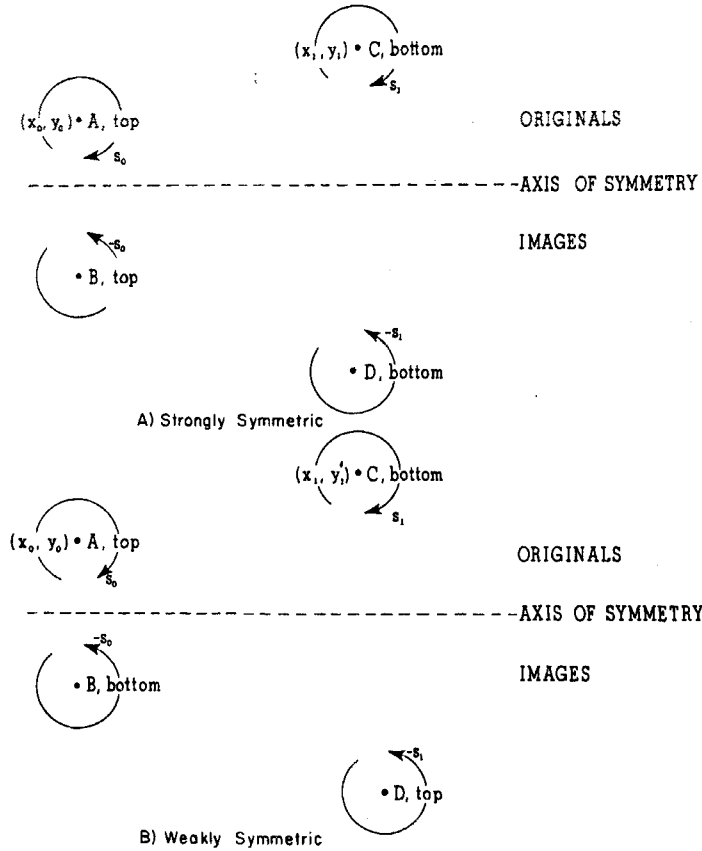


FIGURE 9 This illustrates the two different types of image problem. (A) The strongly symmetric case where the images are in the same layer as the originals. (B) The weakly symmetric case where the images are in different layers than the originals.

These two dichotomies generate four different cases and to compactly present results I've resorted to a tabular presentation: see Table I. The notation is:

$$r_A = [(x - x_A)^2 + (y - y_A)^2]^{1/2} \text{ etc.}$$

= distance from vortex A to the field point  $(x, y)$ ,

$$\begin{aligned}
r_{AB} &= [(x_B - x_A)^2 + (y_B - y_A)^2]^{1/2} \text{ etc.} \\
&= \text{distance between vortices A and B,} \\
\alpha(r) &= \frac{1}{2}[\ln(r) - K_0(r)], \quad \beta(r) = \frac{1}{2}[\ln(r) + K_0(r)], \\
\alpha_A &= \alpha(r_A/\lambda) \quad \text{and} \quad \alpha_{AB} = \alpha(r_{AB}/\lambda) \text{ etc.}
\end{aligned} \tag{4.1}$$

The energy integral  $W$  in (2.8) is given in Table I. Because of the symmetry, (2.2) and (2.6) are degenerate while (2.3) is

$$s_0 y_0 + s_1 y_1 = \text{constant}, \tag{4.2}$$

where  $y_0$  is the ordinate of vortex  $A$  and  $y_1$  is the ordinate of vortex  $C$  (see Figure 9).

### Collisions between pairs of baroclinic vortices

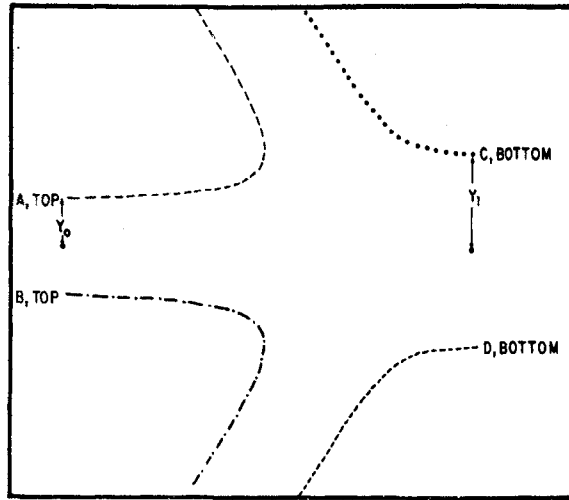
The four different cases in Table I, together with the possibility of varying  $s_0/s_1$ , presents such a variety of possibilities that detailed discussion of all the various cases is beyond the scope of this paper.

Instead I shall focus on a particular interaction: a collision between two pairs which are initially separated by a great distance and are moving directly towards each other. Thus the initial separation of vortices  $A$  and  $C$  in Figure 9 is very large. For instance, Figure 10 shows a collision between a top pair and a bottom pair and it is clear that there are qualitative changes in behavior as the various external parameters are altered. In particular if the initial pairing is disrupted, and partners are exchanged, then energy is converted from kinetic to potential or vice versa. Thus, in Figure 10, if the initial pairs are disrupted, then two hetons are created, and the potential energy of the system has increased.

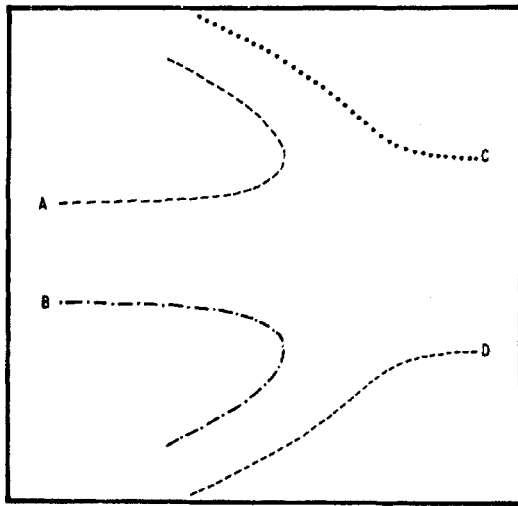
For simplicity I suppose throughout that

$$s_0/s_1 = -1 \tag{4.3}$$

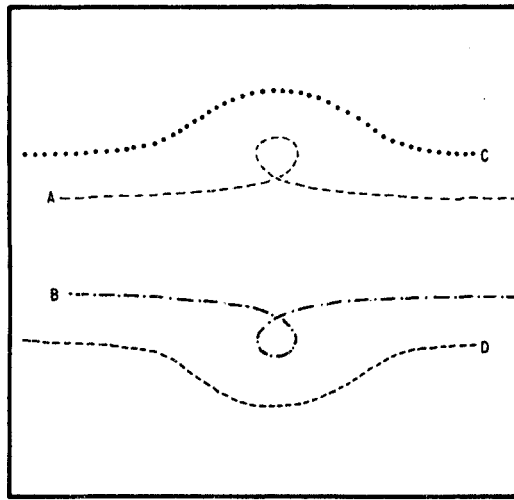
and I shall first discuss a collision between two *barotropic* pairs. It is shown below that the baroclinic problem reduces to the barotropic



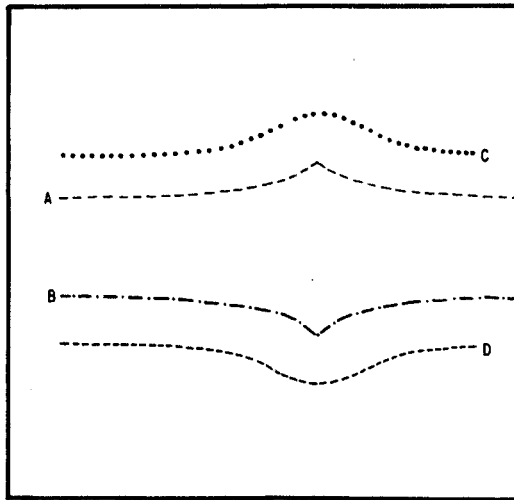
A)  $y_0/y_1 = 2, y_0/\lambda = 0.75$



B)  $y_0/y_1 = 2, y_0/\lambda = 0.60$



C)  $y_0/y_1 = 2$ ,  $y_0/\lambda = 0.55$



D)  $y_0/y_1 = 2$ ,  $y_0/\lambda = 0.50$

FIGURE 10 A numerical integration showing a collision between a top pair and bottom pair. The initial positions are indicated by the labels. In all cases  $y_0/y_1=2$  and the parameter  $y_0/\lambda$  is varied. When this parameter is larger than a critical value there is an exchange of partners while if it is smaller than there is a "slip-through" collision in which the initial alliances are preserved.

TABLE I

The streamfunctions and energy integrals (see 2.8) in the four different cases. The notation is explained in (4.1).

	Strongly symmetric (images in same layer as originals)	Weakly symmetric (images in different layer than originals)
Originals both in top layer	$\psi_1 = s_0\alpha_A - s_0\alpha_B + s_1\alpha_C - s_1\alpha_D$ $\psi_2 = s_0\beta_A - s_0\beta_B + s_1\beta_C - s_1\beta_D$ $W = s_0^2\alpha_{AB} + s_1^2\alpha_{CD} + 2s_0s_1\alpha_{AD} - 2s_0s_1\alpha_{AC}$	$\psi_1 = s_0\alpha_A - s_0\beta_B + s_1\alpha_C - s_1\beta_D$ $\psi_2 = s_0\beta_A - s_0\alpha_B + s_1\beta_C - s_1\alpha_D$ $W = s_0^2\beta_{AB} + s_1^2\beta_{DC} - 2s_0s_1\alpha_{AC} + 2s_0s_1\beta_{AD}$
Originals in different layers	$\psi_1 = s_0\alpha_A - s_0\alpha_B + s_1\beta_C - s_1\beta_D$ $\psi_2 = s_0\beta_A - s_0\beta_B + s_1\alpha_C - s_1\alpha_D$ $W = s_0^2\alpha_{AB} + s_1^2\alpha_{DC} + 2s_0s_1\beta_{AD} - 2s_0s_1\beta_{AC}$	$\psi_1 = s_0\alpha_A - s_0\beta_B + s_1\beta_C - s_1\alpha_D$ $\psi_2 = s_0\beta_A - s_0\alpha_B + s_1\alpha_C - s_1\beta_D$ $W = s_0^2\beta_{AB} + s_1^2\beta_{DC} - 2s_0s_1\beta_{AC} + 2s_0s_1\alpha_{AD}$

when

$$(y_0 - y_1)/\lambda \gg 1. \quad (4.4)$$

For the barotropic problem, with (4.3), the energy integral is

$$W = \frac{1}{2} \ln [r_{AB} r_{DC} r_{AC}^2 / \lambda^2 r_{AD}^2], \quad (4.5)$$

and (4.2) is

$$(y_0 - y_1)/\lambda = c, \quad (4.6)$$

where  $c$  is a constant which, without loss of generality, is positive.

The two integrals (4.3) and (4.4) are sufficient to determine the paths of the vortices A and C relative to each other: this is because  $x_0$  and  $x_1$  appear only in the combination  $x_0 - x_1$  in (4.5). This suggests that "collision coordinates",

$$\xi = (x_0 - x_1)/\lambda, \quad \eta = (y_0 + y_1)/\lambda, \quad (4.7)$$

will simplify the analysis. Note that  $\eta \geq c$ . Using (4.7) the vortex separations are

$$\begin{aligned} r_{AB} &= 2y_0 = \lambda(\eta + c), & r_{CD} &= 2y_1 = \lambda(\eta - c), \\ r_{AC} &= \lambda(\xi^2 + c^2)^{1/2}, & r_{AD} &= \lambda(\xi^2 + \eta^2)^{1/2}, \end{aligned} \quad (4.8)$$

and (4.5) is

$$W = \frac{1}{2} \ln [(\eta^2 - c^2)(\xi^2 + c^2)/(\xi^2 + \eta^2)]. \quad (4.9)$$

Now as  $\xi \rightarrow \pm \infty$  the curves in (4.9) approach horizontal asymptotes  $\eta = \eta_\infty$ , in the  $(\xi, \eta)$ -plane: see Figure 11. It is convenient to use  $\eta_\infty$ , rather than  $W$ , to label the curves. Thus

$$W = \frac{1}{2} \ln [\eta_\infty^2 - c^2] = \frac{1}{2} \ln [(\eta^2 - c^2)(\xi^2 + c^2)/(\xi^2 + \eta^2)]. \quad (4.10)$$

As shown in Figure 11 a curve which is asymptotic to  $\eta = \eta_\infty$  can either (i) approach a vertical asymptote as  $\xi$  decreases, or (ii) cross the  $\eta$ -axis at  $\eta_0$  as  $\xi$  decreases. The first case corresponds to an

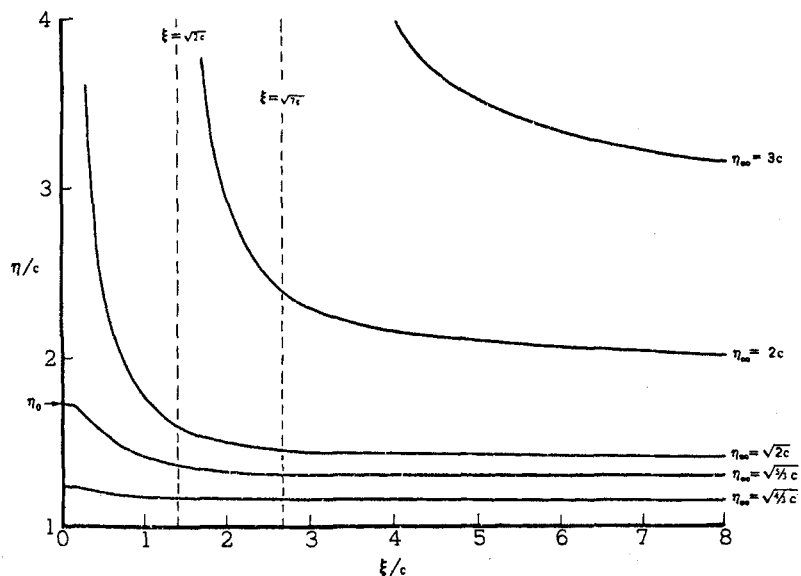


FIGURE 11 Contours of the function  $W$  defined in (4.10). As  $\xi$  becomes large these curves approach horizontal asymptotes:  $\eta = \eta_\infty$ . As  $\eta$  decreases the curves either cross the  $\eta$ -axis or approach vertical asymptotes. For the barotropic case shown above the value of  $\eta_\infty$  which separates the two possibilities is  $2^{1/2}c$ .

exchange of partners because the separation,  $\xi = x_0 - x_1$ , approaches a constant value while  $\eta = y_0 + y_1$  goes to infinity. The second case corresponds to an interaction in which the pairs pass through each other and the initial partnerships are preserved. This is because the separation  $\xi$  approaches infinity and  $\eta$  also returns to its initial value as  $t \rightarrow \infty$ .

The value of  $\eta_\infty$  which separates the two cases will be denoted by  $\eta_*$ . It can be calculated by noting that when  $\eta_\infty = \eta_*$  then  $\eta_0 = \infty$ . Thus putting  $\xi = 0$  and  $\eta = \infty$  into the right-hand side of (4.10b)

$$\ln [\eta_*^2 - c^2] = \ln c^2, \quad (4.11)$$

or

$$\eta_* = 2^{1/2}c. \quad (4.12)$$

The condition (4.12) implies

$$y_0/y_1 = (2^{1/2} + 1)^2 = 5.83, \quad (4.13)$$

i.e., if the ratio of  $y_0$  to  $y_1$  is initially greater than 5.83, then the pairs pass through each and the initial partnerships are preserved.

Analogous considerations apply to the baroclinic problem. As  $\xi \rightarrow \infty$  the curves of constant  $W$  in Table I approach horizontal asymptotes which define  $\eta_\infty$ . Again there is a critical value of  $\eta_\infty$ , denoted by  $\eta_*$ , such that if  $\eta_\infty < \eta_*$  then the curves of constant  $W$  cross the line  $\xi = 0$  at  $\eta_0$ . Vortex pairs with this initial condition preserve their initial partnerships.  $\eta_*$  can be calculated by finding the value of  $\eta_\infty$  such that  $\eta_0 = \infty$ . This leads to a transcendental equation analogous to (4.11). The various cases are listed in Table II together with the qualitative behavior for large and small  $c$ . Note that as  $c \rightarrow \infty$  all four cases reduce to (4.11), i.e. the barotropic problem is recovered when the ordinates of the vortices are separated by a large number of deformation radii.

Figure 12 shows the results of numerically solving the transcendental equation in Table II. Any initial condition is a point on this plane and if it lies *below* the appropriate curve then the partnerships are disrupted when the pairs collide. The barotropic "watershed"

TABLE II

The transcendental equations, analogous to (4.11), which are solved numerically to determine  $\eta_*$  as a function of  $c$ . Also indicated is the behaviour of  $\eta$  as  $c$  decreases from infinity. In the right hand column there is no solution if  $c$  is less than the stated value.

	Strongly symmetric	Weakly symmetric
Originals both in top layer	$\alpha(\eta_* + c) + \alpha(\eta_* - c) = 2\alpha(c)$ $\Rightarrow \eta_* \rightarrow \begin{cases} 2^{1/2}c & \text{as } c \rightarrow 0 \\ 2^{1/2}c & \text{as } c \rightarrow \infty \end{cases}$	$\beta(\eta_* + c) + \beta(\eta_* - c) = 2\alpha(c)$ $\Rightarrow \eta_* \rightarrow \begin{cases} c & \text{as } c \rightarrow 2.54 \\ 2^{1/2}c & \text{as } c \rightarrow \infty \end{cases}$
Originals in different layers	$\alpha(\eta_* + c) + \alpha(\eta_* - c) = 2\beta(c)$ $\Rightarrow \eta_* \rightarrow \begin{cases} 1.43 & \text{as } c \rightarrow 0 \\ 2^{1/2}c & \text{as } c \rightarrow \infty \end{cases}$	$\beta(\eta_* + c) + \beta(\eta_* - c) = 2\alpha(c)$ $\Rightarrow \eta_* \rightarrow \begin{cases} c & \text{as } c \rightarrow 1.55 \\ 2^{1/2}c & \text{as } c \rightarrow \infty \end{cases}$

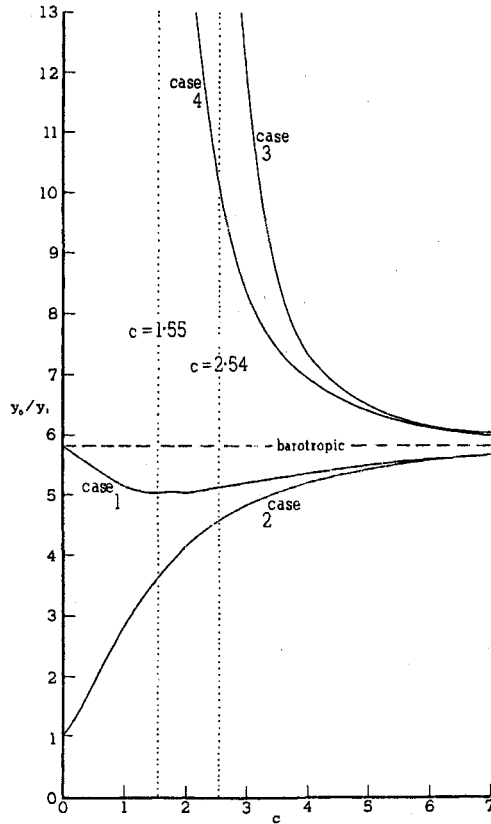


FIGURE 12 This figure summarizes the numerical solution of the various transcendental equations in Table II. Any initial condition can be located as a point in the  $(y_0/y_1, c)$ -plane and classified in one of the four cases. If this point lies above the appropriate "watershed" curves shown above then the initial alliances are preserved, i.e. the pairs "slip through" each other.

(4.13) is simply a horizontal line on this figure, i.e., barotropic dynamics depend only on the initial value of  $(y_0/y_1)$  and are unaffected by variations in  $c$ .

### Case 1 Strongly symmetric and originals in same layer

In this case all four vortices are in the same layer—say the top.

Figure 12 shows that baroclinicity slightly strengthens the bond between partners, i.e. the watershed curve is depressed below the barotropic case so that a wider range of initial conditions preserve original alliances.

### **Case 2 Strongly symmetric and originals in different layers**

In this case a top pair collides with a bottom pair. As one anticipates intuitively, the original pairings are much more robust in this case. In fact even if  $y_0 = y_1$  it is possible for the pairs to “slip through” each other. This is not readily apparent from Figure 12 which collapses the limit  $y_0 \rightarrow y_1$  to a single point. However, the numerical solution shows that if  $\eta_\infty$  is less than 1.42 then the pairs “slip through”.

### **Case 3 Weakly symmetric and originals in same layer**

In this case two hetons collide and may produce two same layer pairs unless  $(y_0/y_1)$  and  $c$  are rather large. In fact Figure 12 shows that the initial hetons are always split (i.e. no matter how large  $y_0/y_1$ ) if  $c$  is less than 2.54. Of the four different cases, this particular collision is most conducive to partner exchange and the splitting decreases the potential energy of the system.

### **Case 4 Weakly symmetric and originals in different layers**

Again two hetons collide but in this case an exchange of partners produces hetons rather than same layer pairs. Figure 12 shows that the initial hetons are always split (i.e. no matter how large  $y_0/y_1$ ) if  $c$  is less than 1.55.

## **5. CONCLUSION**

Our intuitive understanding of vortex dynamics is largely inherited from the classical studies of barotropic vortices. The baroclinic generalization has an external length scale (the Rossby radius of

deformation) which enriches the familiar phenomenology of vortex dynamics in ways which may confound our classical intuition.

For example, perhaps the most remarkable result in the present note is that two colliding hetons will split, no matter how extreme the *ratio* of the breadths of the pairs, provided the deformation radius is sufficiently small relative to the *difference* of the breadths, e.g. Figure 12. In the barotropic problem the outcome of the interaction is determined solely by the ratio and if this is sufficiently large splitting does not occur.

The transport of fluid associated with a baroclinic pair is also noteworthy. A top pair transports no lower layer fluid if the spacing between the vortices is less than 1.72 deformation radii. By contrast the extent of the trapped region in both layers associated with a heton increases without bound as the spacing decreases.

This result is analogous to Stommel and Hogg's observation that the heat transport of a heton increases as the spacing decreases. The physical explanation is straightforward: as the translation speed of the heton decreases weak, far field velocities are sufficient to drag fluid along with the pair. This also leads one to speculate that a heton with small spacing will be strongly perturbed by the  $\beta$ -effect: north-south motion of the heton will carry a large volume of fluid through the planetary vorticity field. Consequently relative vorticity will be generated in a large volume of fluid which envelopes the heton. It seems unlikely that this effect can be approximated using the modulated vortex method which Zabusky and McWilliams (1982) applied successfully to the barotropic problem.

### Acknowledgements

I thank Nelson Hogg, Henry Stommel and Chris Wooding for stimulating discussions and allowing me to use their heton programs. This research was supported by ONR Grant N00014-79-C-0472. Contribution of the Scripps Institution of Oceanography, new series.

### References

- Acton, E., "The modelling of large eddies in a two-dimensional shear layer," *J. Fluid Mech.* **76**, 561-592 (1967).
- Aref, H., "Integrable, stochastic and turbulent vortex motion in two-dimensional flows," *Ann. Rev. Fluid Mech.* **15**, 345-389 (1983).

- Batchelor, G. K., *An Introduction to Fluid Mechanics*, Cambridge University Press (1967).
- Hogg, N. and Stommel, H., "The heton, an elementary interaction between discrete baroclinic geostrophic vortices, and its implications concerning eddy heat-flow," Submitted to *Proc. Roy. Soc. A* (1984a).
- Hogg, N. and Stommel, H., "Heton explosions: the breakup and spread of warm pools as explained by baroclinic point vortices," in preparation (1984b).
- Lamb, H., *Hydrodynamics*, Dover, New York (1932).
- Love, A. E. H., "On the motion of paired vortices with a common axis," *Proc. London Math. Soc.* **25**, 185-194 (1894).
- Pedlosky, J., *Geophysical Fluid Dynamics*. Springer-Verlag (1979).
- Zabusky, N. J. and McWilliams, J. C., "A modulated point-vortex model for geostrophic,  $\beta$ -plane dynamics," *Phys. Fluids* **25** (12), 2175-2182 (1982).